Supporting Information for "A multi-sensor approach for the characterization of tropical cyclone induced swell - Application to TC Larry, 2021"

Clément Pouplin[1], `https://orcid.org/0009-0002-9991-6424`, **Alexis Mouche**[2], `https://orcid.org/0000-0003-1250-4436`, **Bertrand Chapron**[2], `https://orcid.org/0000-0001-6088-8775`

[1]France Energies Marines, 525 Av. Alexis de Rochon, 29280 Plouzané, France
[2]Institut Francais de Recherche pour l'Exploitation de la Mer (IFREMER), 1625, route de Sainte-Anne, Plouzane, 29280, France

Introduction

This documents provides Supporting Information related to "A multi-sensor approach for the characterization of tropical cyclone induced swell - Application to TC Larry, 2021". In this document, details related to data and methodology are presented in sections 1 and 2 respectively. In section 3 and 5, other examples of directional wavelength distributions are described. Sections 4, 6 and 7 provide supplementary information about the parametric wave models considered in this study. In section 8, variables composing the datasets provided are presented in tables.

S1 Data and model hindcast

The data and model hindcast considered in this study are further detailed in this section.

S1.1 Wave data

S1.1.1 Sentinel-1 SAR (Wave Mode) - ESA Level62 OCN products

The Copernicus/ESA Sentinel-1 mission is a constellation of two polar-orbiting satellites with a C-band Synthetic Aperture Radar (SAR), enabling them to acquire imagery day and night regardless of the weather. Sentinel-1 A and Sentinel-1 B have been launched in April 2014 and April 2016, respectively, and operate with four exclusive acquisitions modes. The wave mode (WV) is the default one over open ocean. In this mode SAR images are acquired every 100 km at two alternating incidence angles (23.5° and 36.5°) and in single VV polarization (default). Each SAR WV image is about 20x20 km with 5 m spatial resolution.

All Sentinel-1 WV data acquired over oceans (including seas) are systematically processed up to Level-2 Ocean product (L2 OCN). The OSW (ocean swell) component of the OCN product provides the two-dimensional ocean surface wave spectrum estimated by inversion of the corresponding image cross-spectra (Engen & Johnsen, 1995). This 2 dimensional wave spectrum is separated into up to 5 wave systems, called "partitions". In this study we rely exclusively on the peak wavelength, the peak direction and the significant wave height processed for each partition, from the OSW component of the Level-2 OCN product to monitor the swell systems outrunning from TCs. The peak direction is sometimes provided with a 180 degrees ambiguity that is removed in our pre-filtering step (cf first step of the algorithm description in section 3).

Corresponding author: Clément Pouplin, `clement.pouplin@france-energies-marines.org`

Wave Mode (WV) is continuously operated over open oceans, with lower priority versus the other modes with larger swaths. For example, European waters including the north-east Atlantic ocean basin are not observed with WV mode to take benefit of wide swath modes for ship, oil-spill and sea-ice detection applications. Overall, Sentinel-1 constellation acquires about 120k imagettes per month in WV mode allowing for a nearly-global monitoring of the waves in open oceans. Figure S1 illustrates the coverage obtained with 20k Wave Mode acquisitions during a repeat cycle (12 days and 175 orbits per cycle for a each satellite). As expected, most of the coastal areas and the north-east Atlantic basin are not covered by the WV mode.

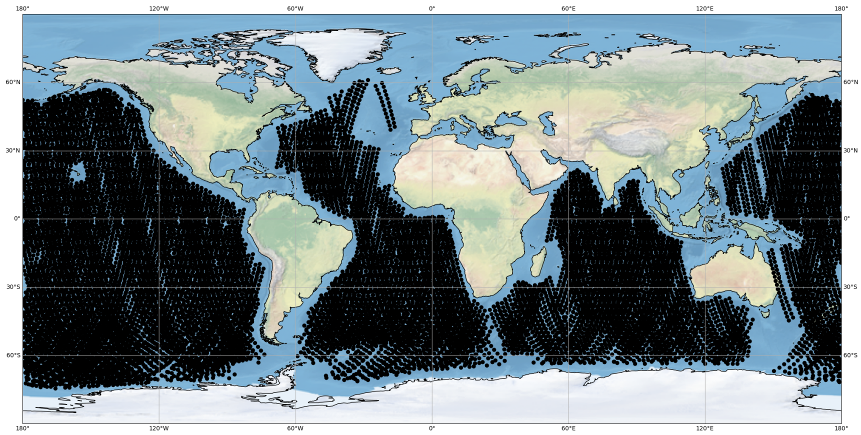

Figure S1. Location of Wave Mode acquisitions during a full cycle of Sentinel-1 A, between 2021-05-30 and 2021-06-10. 20 070 SAR acquisitions were made during this cycle.

The SAR instrument uses the motion of its satellite platform to achieve high resolution images. However, motions of the ocean surface waves during the integration time disturb the along track resolution (Stopa et al., 2015). This phenomenon translates into a specific wavelength (called azimuth cutoff wavelength) below which no energy can be acquired. This limitation, inherent to all SAR systems is sea-state dependent and even more important when the local wind is strong. This is why this study relies on Sentinel-1 only for swell monitoring outside the storm area.

S1.1.2 CFOSAT SWIM - L2S product

Launched in october 2018, CFOSAT is a satellite mission resulting from a partnership between the French (CNES) and China (CNSA) space agencies, aiming at characterizing jointly the waves and wind in open ocean, with 2 different sensors onboard. SCAT is a Chinese Ku-band scatterometer operating at mid incidence angles for ocean surface wind vectors measurement and SWIM is a French Ku Band Real Aperture Radar spectrometer operating at low incidence angles for 2D ocean wave spectra, significant wave height and sea level measurement. The SWIM acquisitions are performed thanks to 6 rotating beams, allowing for alternate measurements at 6 different incidence angles : 0, 2, 4, 6, 8 and 10 degrees from nadir. The resulting footprint pattern of this acquisition mode is a combination of 5 distinct and intertwined cycloids, one for each angle of incidence, in addition to a nadir beam. Each near-nadir acquisition provides a 1D ocean wave spectrum in the azimuth direction of the beam with a footprint of about 18 km in diameter.

Based on this acquisition pattern, the so called "L2S" product provides information on the wave systems measured by SWIM. For each beam separately, all the directional 1D wave spectra obtained along the cycloid track are concatenated in time, to obtain two dimensional "ribbons" (time, wavenumber). The L2S product synthesizes these ribbons into a list of detected wave partitions described by peak wavelength, peak direction and significant wave height, that are considered in our study (CNES, 2017). The peak direction is provided with a 180 degree ambiguity that has to be removed in the first step of the algorithm description in section 3.

On figure S2, the footprint of the beam with an incidence of 6 degrees on 2021-01-20 at 07:39 AM is spatially scattered on the map, and the corresponding 1 dimensional spectra are concatenated on the left hand side. Swell systems are surrounded by corresponding colored ellipses both on the map and on the ribbon. In this example, two systems are visible, one is directed along the west-east axis and is approximately 420 m long (the wavenumber is approximately equal to 0.015 m^{-1}). This wave system is surrounded by the grey and white ellipses. Another system propagates towards NNW or SSE, approximately 200 m long, and surrounded by orange and red circles.

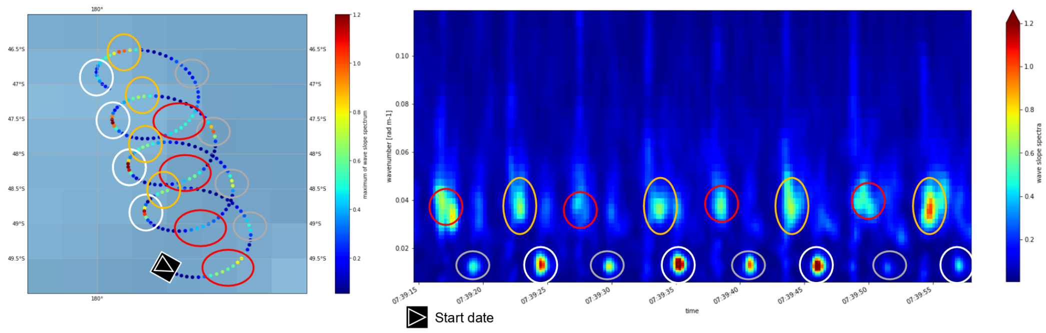

Figure S2. (Left) track of the cycloid footprint for the 6 degrees beam. (Right) Wave slope spectrum corresponding to this ribbon.

The coverage of CFOSAT is global, upon every seas and oceans. However, SWIM measurements are strongly impacted by rain, such that their accuracy is expected to be lowered to measure waves inside storms and tropical cyclones.

S1.1.3 Sofar Ocean Spotter drifting buoys

Sofar is a private company developing drifting metocean buoys called Spotter (Houghton et al., 2021). This study relies on a global dataset of 663 buoys, with measurements spanning from October 2020 to November 2021. These buoys provide 2 dimensional wave spectra with temporal resolution of 1 hour. The network coverage (location of each buoy) on 09/27 (as an example) is presented on figure S3 below.

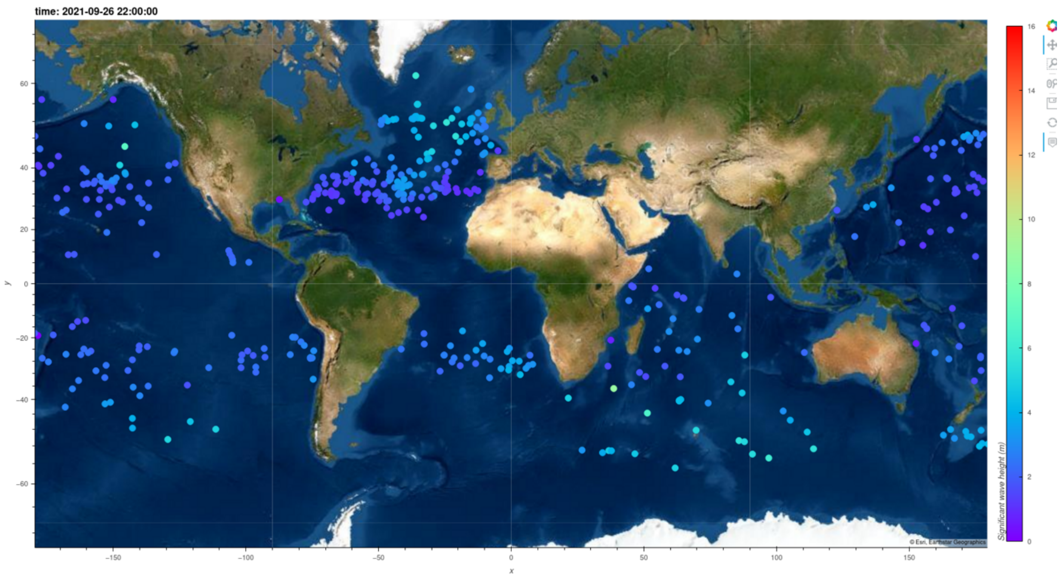

Figure S3. Coverage of Spotter buoys on 09/27. Each dot represents a Spotter buoy, the color of each dots is the significant wave height at buoy location on 09/27.

The method used in order to extract wave systems from these hourly wave spectra is as follows.

1. Sofar Spotter wave spectra are reconstructed using the maximum entropy method (MEM) (Lygre & Krogstad, 1986), with a 3 degree directional resolution.
2. Reconstructed wave spectra are smoothed along the wavenumber axis, using a length 5 uniform kernel. As the MEM applies to each wavenumber independently, this operation is necessary to remove the noise before partitionning.
3. A partitioning method using Hanson's watershed algorithm (Hanson et al., 2009) is applied to extract the peaks corresponding to different wave systems.
4. If some peaks are too close enough in terms of spectral distance (cf section S1.3 in SI for spectral distance definition), they are grouped into the same wave system.

The peak direction, peak period and significant wave height of wave systems extracted from each hourly spectra from each buoy are considered in this study. Peak periods are then converted to peak wavelengths through the deep water dispersion relationship, to make them consistent with satellite observations. In shallow and intermediate water depth, the bathymetry will make the group velocity change. Yet, waves spend the most important part of their trajectory in deep water areas, such that the true back propagation trajectories (taking the bathymetry into account) will be close to our deep water hypothesis estimate (around 30 kms at most). Relatively to the co-location criteria with the TC (± 3 hours, disc of radius R_{34} reaching values between 100 and 400 km), the uncertainty on the back propagation trajectory looks very small.

S1.1.4 NDBC buoy network

NDBC is a buoy network operated by NOAA, mainly located along the US coastline (see the coverage on figure S4). As some buoys do not provide wave spectra, the integrated parameters (peak period, mean direction of dominant wave system, and significant wave height) are considered in our study. The temporal resolution of measurements depends on the buoy.

Periods and directions only take discrete values, such that directional distribution of wavelength (wave roses) described in section 4 may not be continuous, especially for wavelength over 250 m, where wavelength bins are about 40 m long.

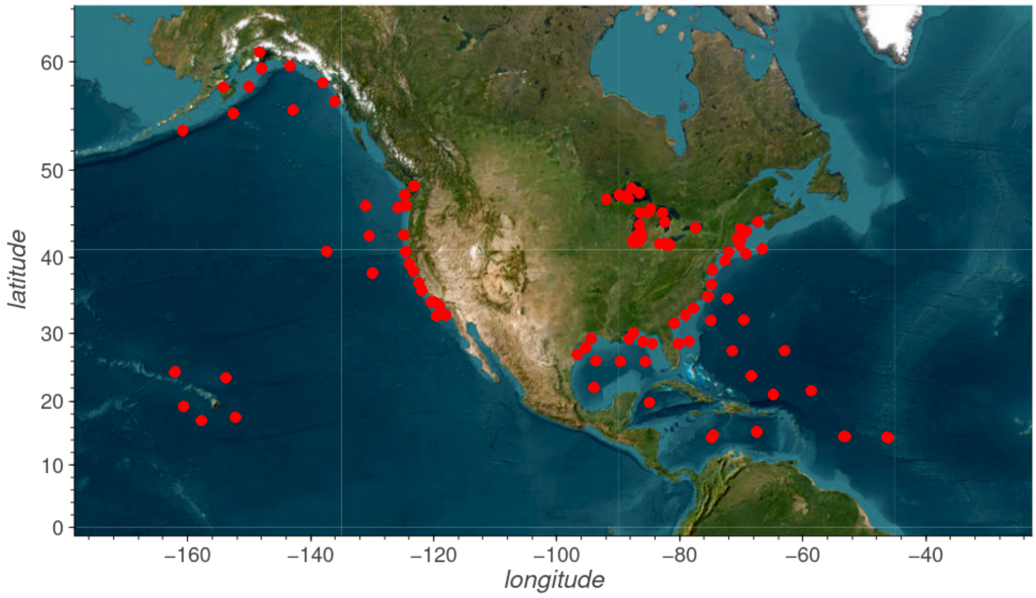

Figure S4. Coverage of NDBC buoys

S1.2 Tropical cyclone data

Tropical cyclone information are obtained from IBTrACS (Knapp et al., 2010). The IBTrACS database describes the evolution of tropical cyclone locations with a temporal resolution of 6 hours. Other variables such as maximum wind speed, translation speed and 34 kts wind radius (defined as the maximum distance to the eye where the wind speed is equal to 34 kts, written R34) are also provided in this product.

The IBTrACS database gathers analyses from different tropical cyclone centers in the world (USA, Japan...). In a synoptic version of IBTrACS, presented in (Ifremer, 2022), the information provided by the centers is merged to get only one common track by TC, interpolated every 3 hours. This version of the IBTrACS database is considered in this study.

S1.3 WAVEWATCH-III ®(WW3) model hindcast

WW3 model hindcasts are considered during the post processing step of the algorithm presented in section 3. The hindcasts are provided on a regular grid with spatial resolution of 0.5 degree and temporal resolution of 3 hours. At each grid point, up to 4 spectral partitions are available, defined by their peak period and direction. WW3 model hindcasts are used in 3 different steps of the algorithm:

1. Remove the 180 degree directional ambiguity for some wave data (CFOSAT SWIM L2S and Sentinel-1 in some cases)

2. Filter out wave systems that are not physical by direct comparisons between observations and model. During the post processing step, the spectral distance (defined below) between an observed wave partition and each partition on the co-located WW3 spectrum is computed. If at least one of the WW3 co-located partitions has a spectral distance lower than 1 with the observed system, it is kept.
3. Filter out observations induced by other meteorological events than the TC. The closest WW3 partition is extracted all along the back propagation trajectory of the observed wave partition, every 3 hours. A comparison between the obtained WW3 global H_s time serie, and matched up partition H_s time serie is then used to eliminate swell systems that crossed the TC but were generated by another windy event (extra tropical storm for example).

In order to compare WW3 and observed wave partitions, a metric called spectral distance, as defined in Husson (2012) is considered. For two partitions $P_{i_1}^{n_1}$ and $P_{i_2}^{n_2}$ from observations n_1 and n_2 of peak period $T_{i_1}^{n_1}$, $T_{i_2}^{n_2}$ and peak directions $\theta_{i_1}^{n_1}$, $\theta_{i_2}^{n_2}$, respectively, the spectral distance $D_{\text{spec}}(P_{i_1}^{n_1}, P_{i_2}^{n_2})$ is:

$$D_{\text{spec}}(P_{i_1}^{n_1}, P_{i_2}^{n_2}) = \frac{1}{q}\left(|\theta_{i_1}^{n_1} - \theta_{i_2}^{n_2}| + r\frac{|T_{i_1}^{n_1} - T_{i_2}^{n_2}|}{T_{i_1}^{n_1} + T_{i_2}^{n_2}}\right) \tag{1}$$

where q and r are constants defined in (Husson, 2012) ($q = 60$, $r = 250$). Peak periods are directly defined from dispersion relation for surface waves in deep ocean.

$$T_i^n = \sqrt{\frac{2\pi g}{\lambda_i^n}} \tag{2}$$

S2 Reliability of elliptical fit

Each elliptical fit performed on the wave roses is associated with a reliability value that depends on the amount of data available and their directional distribution (cf section 4.2). The wave rose is separated into 36 bins of 10 degrees from which the 90^{th} percentile of the wavelength distribution is extracted. The reliability is defined as $R = \frac{D}{E}$. E is the root mean square error between the wave rose of these maximum wavelengths by directional bins, and the fit. D is the data reliability, quantified as a crossed sum of differences between all couples of directional bins where data are available in the wave rose, weighted by the product of the amount of wave data available in each bin. The result is divided by the number of direction bins (36). If n_i is the number of wave observation in the wave rose, in the i^{th} bin with direction ϕ_i, we have:

$$D = \frac{1}{36}\sum_{i=0}^{36}\sum_{j=0}^{36}|\phi_i - \phi_j|n_i n_j \tag{3}$$

The evolution of the root mean square error between the data and the elliptical fits is provided as function of time on figure B.1. The fit error mainly varies between 20 and 60 meters until 09/10. It stabilizes around 30 m at the end of the mature phase (best fits), before increasing up to 100 during the decaying phase of the life cycle.

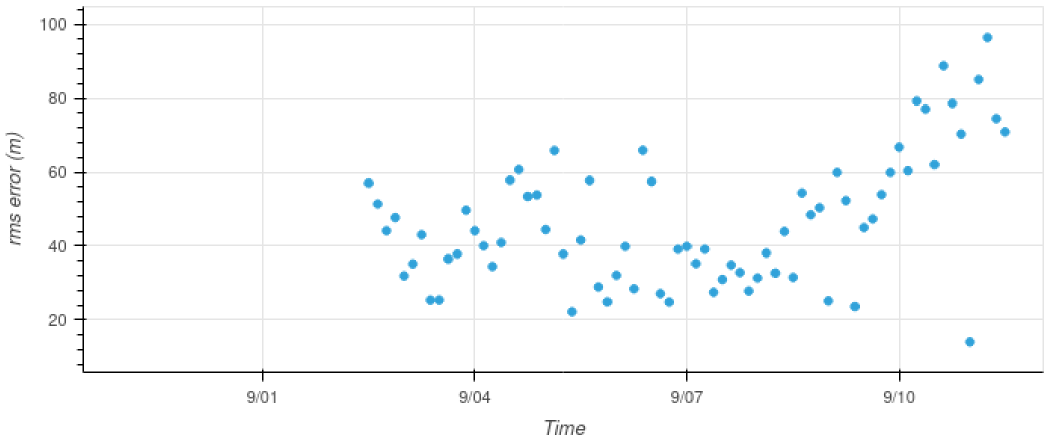

Figure S5. Evolution of the root mean square error of elliptical fits as function of time

S3 Extended wave rose on 09/07 at 9 AM (+/- 3hours)

An extended wave rose is defined as the superimposition of a wave rose at a given time with the wave roses 3 hours before and after. This procedure enriches the wave rose which is useful to examine the integration of swell along satellite orbits, as presented in section 5.2. On figure S6 the extended wave rose corresponding to figure 2 is presented. Sentinel-1 and CFOSAT passes catching waves induced by the TC appear continuous, while discontinuities on the satellite orbits can be observed on figure 2. The directional sector examined in section 5.2 is represented by dotted green curves on both the map and the wave rose. Superimposing wave roses provides more data in this directional sector to analyse the dispersion of TC induced waves. These 3-hours wave roses are also used during the wave rose reduction with an ellipsis (section 4.2), as the reliability of the fits is improved using more data.

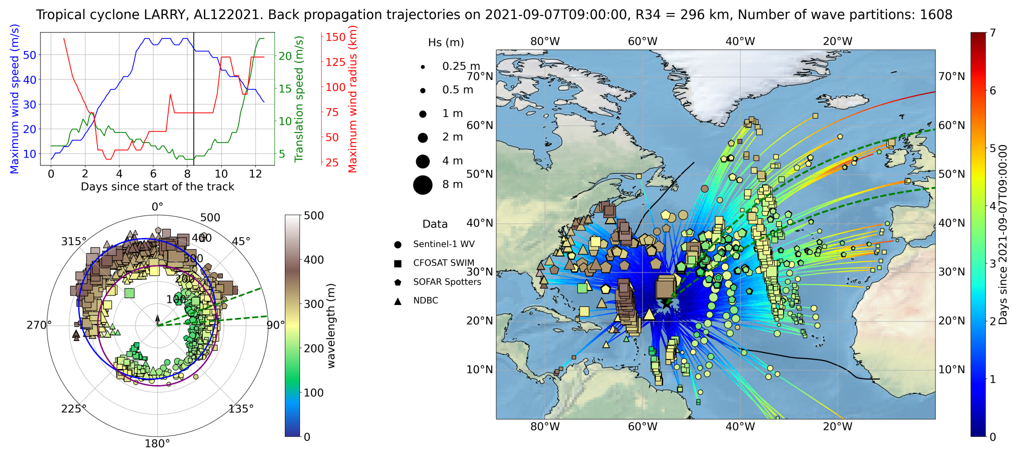

Figure S6. (left) Extended wave rose on 09/07 at 9 AM, (right) map of measurements

S4 Discussion on the wave rose thickness with a parametric model

The thickness observed in the wave rose for the directional sector examined in section 5.2 is discussed. The KYC 2021 parametric Lagrangian wave model (Kudryavtsev et al., 2021a) is used to simulate the variability of the wavelengths leaving the TC towards a given direction. In this model, wave groups are represented by Lagrangian particles called wave rays, forced by a wind field varying in time and space. On figure S7, some wave rays propagating towards the directional range between 70 and 85 degrees are represented and color coded with their wavelength. Directions of propagation of escaping rays do not seem to be included between 70 and 85 degrees on the figure because trajectories are displayed in the referential of the translating tropical cyclone. The colored background represents the wind speed. After being forced by the wind field, the peak wavelength of these wave groups is found to span between 50 and 270 meters approximately. Our data analysis reveals (see on figure 2) that wavelengths between 120 and 300 m are observed. The apparent difference between model and observations for the lower values of wavelength (between 50 and 100 m) is expected as our data analysis focuses only on longer swell systems propagating outside the TC vortex. In the contrary the shorter waves encounter fast dissipation and cannot be observed far from the TC. Moreover, modelled wave rays were forced with a simplified parametric wind profile (Holland) such that wave rays trajectories and final wavelengths are approximative. Overall this simulation exercise illustrates the large range of wavelengths obtained for the waves propagating towards a given directional range.

On figure S7, only a few rays are displayed for the sake of simplicity. By refining the mesh of the initialization locations of the wave groups, as defined on figure 1 in Kudryavtsev et al. (2021b), all the wave rays propagating in the directional sector (70 - 85 degrees) have been initialized in a specific area in the cyclone (delimited by a green dotted contour on figure S7), covering regions with various wind intensities. The variability of the wavelength leaving the TC seems directly related to the variability of the initial wind speed inside this area.

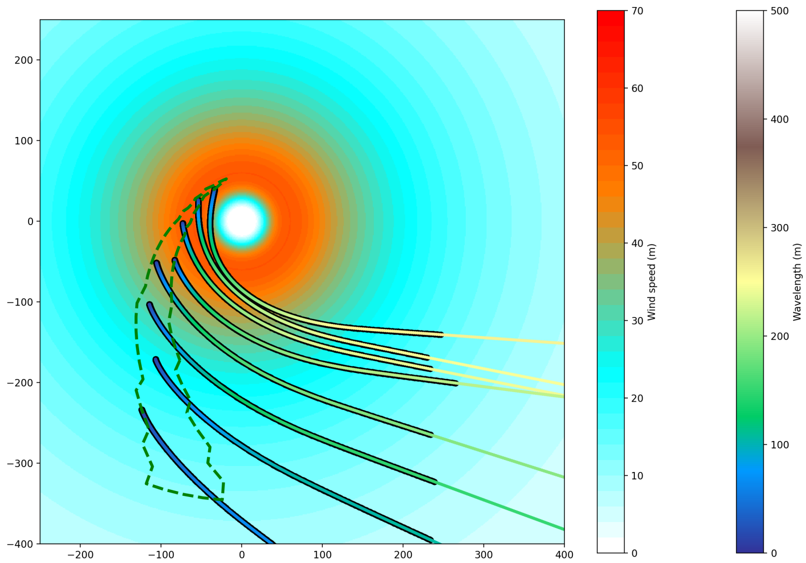

Figure S7. KYC2021 parametric model wave rays in a Holland wind field corresponding to Larry's conditions on 09/07 at 9 AM. The colored background is the Holland wind speed. The color of the curves represents the evolution of the wavelength along the propagation trajectory. External contours of these curves are black at locations where the wind is forcing the waves. The green dotted contour provides the area of initialization of wave rays escaping the tropical cyclone towards 70 to 85 degrees clockwise with respect to its direction of translation.

S5 Other wave roses examples

In this section, 3 particular wave rose cases are discussed.

On figure S8, one of the most front-rear asymetric wave roses during the life cycle of TC Larry is presented (09/03 at 12 PM, during the intensification phase). Most data are captured on the right hand side of the tropical cyclone. As explained in section 5.3, during the beginning of the life cycle, the elliptical fits are less reliable. This case is an example of low reliability (5x10^5), because there is few data on the left hand side and the rear of the TC. A few CFOSAT SWIM data are available on the left hand side, but do not allow to represent the whole directional distribution. These observations are quite isolated on the map, because other measurements performed during the same satellite passes were associated to another TC timestamp or filtered out. On the wave rose, the longest wavelength was acquired towards 30 degrees in the wave rose. However this case provides a ϕ_0 of 0 degree approximately. The lack of data in the left sector makes it difficult to derive ϕ_0, which could actually be negative if some long wavelength values had been acquired from the front left of the TC.

On figure S9 (on the 09/06 at 9 PM, during the mature phase) the wave rose provides a similar ϕ_0 value than on figure S8. However, it has higher reliability (2.8x10^6) because data are available in every directions, which confirms the fact that getting reliable positive ϕ_0 values is physically possible, and can be observed if enough data are available around the TC.

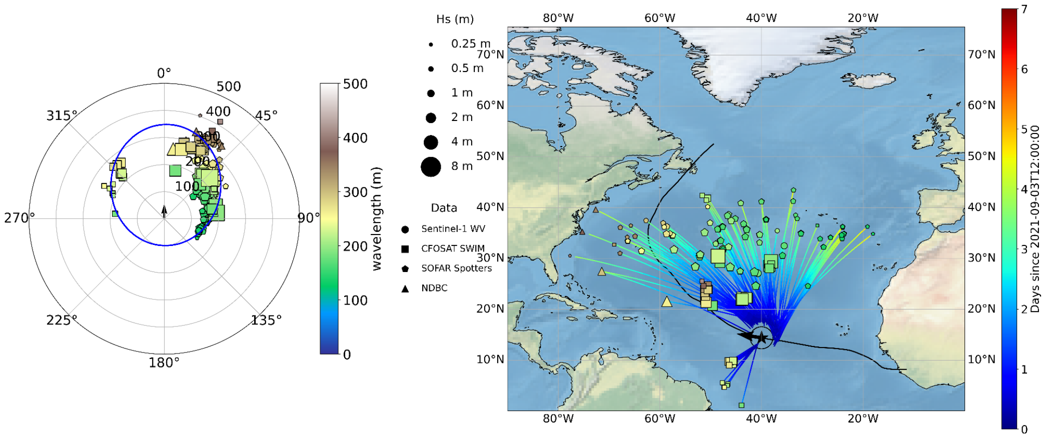

Figure S8. (left) Wave rose on 09/03 at 12 PM, (right) map of observations

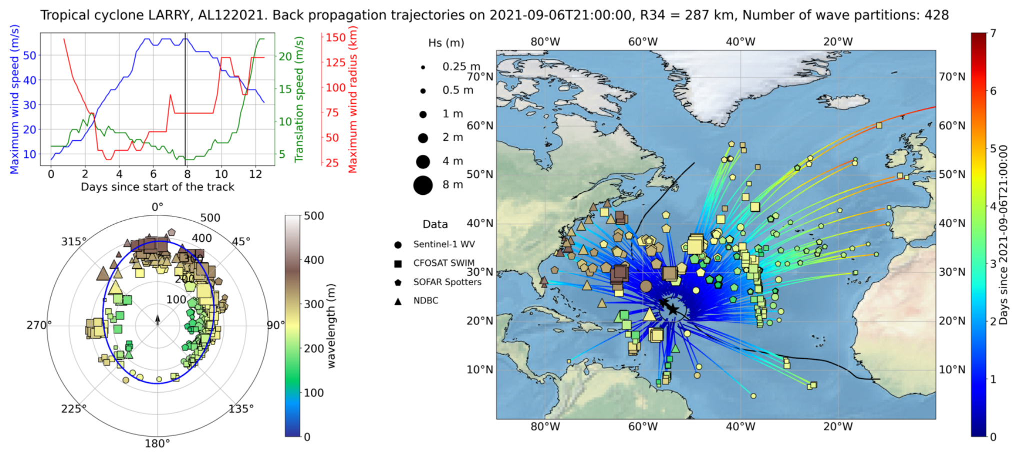

Figure S9. (left) Wave rose on 09/06 at 9 PM, (right) map of observations

The orientation of the wave rose ϕ_0 is expected to characterize the direction of propagation of the longest waves. However in some cases it is strongly influenced by the short wavelengths acquired in the rear quadrants. This phenomenon is illustrated on figure S10 (on 09/05 at 6 AM, during the mature phase). The wave rose is mainly composed of wave measurements propagating from the TC front. A few measurements also catch wave systems coming from the TC right rear. At this timestamp, ϕ_0 is about -25 degrees. However, wavelengths measured by the multi-sensor network are approximately the same between -25 and +5 degrees. In this case, ϕ_0 is likely to be influenced by the direction of the shortest wavelength measurements acquired at this timestamp, which are between 90 and 135 degrees. These short measurements in the right rear sector drive ϕ_0 towards negative values, as this ellipsis methodology forces the longest and shortest wavelengths to be opposed in the wave rose. The shortest wavelength influences ϕ_0 as much as the longest ones, which explains the suddenly low ϕ_0 value on 09/05 at 6 AM, discussed in section 5.3 and presented on figure 4.

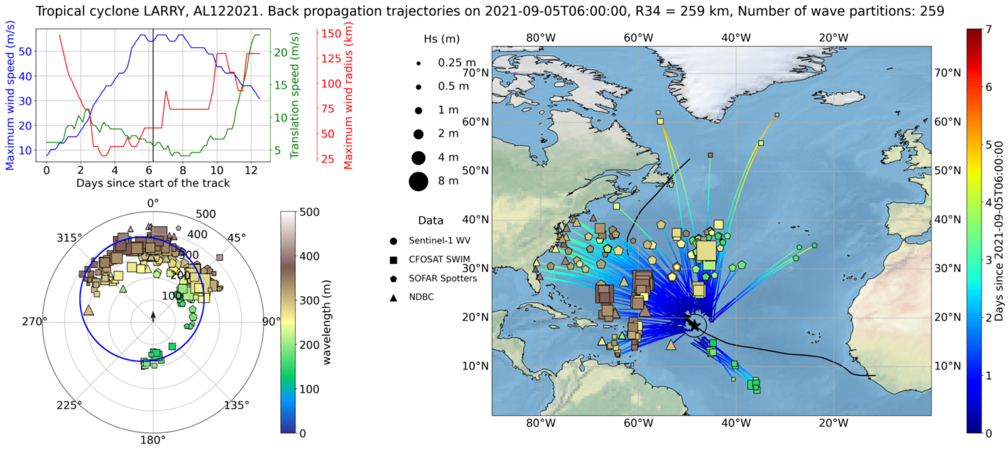

Figure S10. (left) Wave rose on 09/05 at 6 AM, (right) map of observations

S6 Parametric formulation for the extended fetch, from Young and Vinoth, 2013

Young's extended fetch estimation is performed through a polynomial fit between observed significant wave height by altimeters and tropical cyclone vitals. The equivalent extended fetch is defined as function of the TC vitals (I. R. Young, 1988).

$$\frac{F}{R'} = (aV_{\max}^2 + bV_{\max}V_{\mathrm{t}} + cV_{\mathrm{t}}^2 + dV_{\max} + eV_{\mathrm{t}} + f) \tag{4}$$

The equivalent fetch F is the product of

- A two dimensional parabolic function of $V_{\max}$ and V_{t} (with $a = -2.175\ 10^{-3}$, $b = 1.506\ 10^{-2}$, $c = -1.223\ 10^{-1}$, $d = 2.190\ 10^{1}$, $e = 6.737\ 10^{1}$ and $f = 7.98\ 10^{1}$)
- $R' = 22.5\ 10^3 \log_{10} R_{\max} - 70.8\ 10^3$

,

In I. Young & Vinoth (2013), coefficients d, e, and f are modified, taking advantage of significant wave height altimeter data inside tropical cyclones ($d = 8.760\ 10^{-2}$, $e = 1.516$, $f = 1.756$). Moreover, a correction factor defined by I. Young & Burchell (1996) multiplies equation 4 on the right hand side to remove the bias related to $V_{\max}$ and V_{t} ($\lambda = -0.015V_{\max} + 0.0431V_{\mathrm{t}} + 1.30$).

The fetch laws as defined in Kudryavtsev et al. (2021a) can be applied to this fetch in order to compute peak wavelength and significant wave height.

S7 Parametric formulation for the extended fetch, from Kudryavtsev et al. 2015

Kudryavtsev's formulation is an extension of the fetch laws in the case of a translating wind event. In this section, the main equations from appendix A of Kudryavstev et al, 2015 are presented. In this model a steady wind field is considered, and the propagation in the stationnary or translating TC referential is examined. In such a modelling, we assume that on the right hand side of the TC the waves are forced along a quarter circle at a constant distance from the TC center. The wave growth follows the classic fetch laws : $\alpha = c_\alpha \tilde{x}^q$, where α is the wave age, and x is the absolute fetch. The objective is to characterize the TC induced wave growth thanks to two parameters : the maximum wind speed $V_{\max}$ and the TC translation velocity V_{t}.

S7.1 Stationary TC

We first approximate the wave spectrum $E(\omega)$ around the peak ω_p

$$E(\omega) = E(\omega_p) + \frac{1}{2} E''_\omega (\omega - \omega_p)^2 \tag{5}$$

With this expression of $E(\omega)$, the spectrum equation writes :

$$\partial \omega_p / \partial t + (1 - \Delta) c_g \partial \omega_p / \partial x = -\left(S'_\omega / E''_\omega\right)_{\omega = \omega_p} \tag{6}$$

As $\Delta = \left(\omega_p E'_{\omega_p}\right) / \left(\omega^2 E''_\omega\right)\big|_{\omega=\omega_p}$ is much smaller than 1, and assuming, with respect to self-similarity concept, that $(S'_\omega / E''_\omega)_{\omega=\omega_p} = -(g/u)^2 \varphi(\alpha)$, where $\varphi(\alpha)$ is a dimensionless universal function of the wave age, and u the wind speed :

$$\partial \omega_p / \partial t + c_g \partial \omega_p / \partial x = (g/u)^2 \varphi(\alpha) \tag{7}$$

We obtain a generalized equation for wind wave growth in a wind field depending on space and time. In order to get the know fetch law for stationary conditions $\partial \omega_p / \partial t = 0$, we obtain:

$$\varphi(\alpha) = 1/2 q c_\alpha^{1/q} \alpha^{-1/q} \tag{8}$$

S7.2 Translating TC

For a translating TC, equation 7 becomes:

$$\left(c_g - V_{\mathrm{t}}\right) \partial \omega_p / \partial X = (g/u)^2 \varphi(\alpha) \tag{9}$$

With $X = x - V_{\mathrm{t}} t$ and $u(x,t) = uH(x - Vt)$. Taking into account 8,

$$\frac{\partial \alpha}{\partial \tilde{X}} = q c_\alpha^{1/q} \alpha^{(1-1/q)} \left(\frac{u}{u - 2\alpha V_{\mathrm{t}}} \right) \tag{10}$$

After integration,

$$\alpha^{1/q} (1 - (2V_{\mathrm{t}}/u)(1+q)^{-1} \alpha) = c_\alpha^{1/q} \tilde{X} + C \tag{11}$$

The integration constant C can be found such that when $\tilde{X} = 0$, $c_g^p = V$. $\tilde{X} = 0$ is then chosen by convention as the location, in the moving frame of reference, where the wave acquired a sufficient energy to reach the TC translation speed. Then equation 11 becomes, introducing $\alpha_T = u/2V$,

$$\alpha^{1/q} (1 + q - \alpha/\alpha_T) - q \alpha_T^{1/q} = (1+q) c_\alpha^{1/q} \tilde{X}. \tag{12}$$

The position of the generation of the waves that encountered the maximum wind energy can be found where $\alpha = \infty$. This location is the critical fetch L_{cr}, the distance that is necessary in the translating TC referential to reverse the wave direction with respect to TC motion (because we set the location where $c_g = V$ at $\tilde{X} = 0$):

$$\tilde{L_{cr}} = -c_\alpha^{1/q} \frac{q}{1+q} \alpha_T^{1/q} \tag{13}$$

As expected, if V=0, $\tilde{L_{cr}} = 0$. The complete wave development equation is:

$$\alpha^{1/q}(1 - (1+q)^{-1}\alpha/\alpha_T) = c_\alpha^{1/q}(\tilde{X} - \tilde{L_{cr}}) \tag{14}$$

In the case of waves propagating in the direction opposite to TC motion, equation 11 can be rewritten considering $\alpha = \infty$ when X = 0

$$\alpha^{1/q}(1 - (1+q)^{-1}\alpha/\alpha_T) = c_\alpha^{1/q}\tilde{X} \tag{15}$$

S7.3 Effective fetch calculation

The objective of this section is to compute theoretically the extended fetch of the most energetic waves as function of $V_{\max}$, $R_{\max}$ and V_{t}. We consider the wind is blowing on the right hand side of the translating TC, on a distance $l = \frac{\pi}{2} r$, where r is the distance to the TC center. We assume that the longest waves are generated close to the radius of maximum winds, with the maximum wind speed, such that $r = R_{\max}$ and $u = V_{\max}$. The method is as follows, it is different for slow ($l > L_{\mathrm{cr}}$) and fast ($l < L_{\mathrm{cr}}$) TCs :

S7.3.1 Slow TCs

First, let us consider cases where $\frac{\pi}{2} R_{\max} > L_{cr}$, ie cases where the TC reverses the wave group direction with respect to TC translation at some location. In such cases, the wave group leave the TC by the front, at $\tilde{X} = lg/V_{\max}^2$. We use this value of $\tilde{X}$ in equation 14.

A fourth order polynomial equation in α is obtained assuming q = -1 / 4.

$$\alpha^4 = c_1 \alpha + c_2 \tag{16}$$

With $c_1 = -c_\alpha^4 V_{\max}^2/((l - L_{\mathrm{cr}}) g \alpha_T (1+q))$ and $c_2 = c_\alpha^4 V_{\max}^2/((l - L_{\mathrm{cr}}) g)$

We can use Ferrari's method to solve this fourth order equation. Two real solutions can be obtained The two other solutions are non real and not considered. Getting only two real solutions was expected as the direction of waves with respect to TC translation can only be reversed once, then for a same $\tilde{X}$, only one or two α solutions can be found.

$$\alpha_{1,2} = \frac{a_0 \pm \sqrt{a_0^2 - 4(t_0 - b_0)}}{2} \tag{17}$$

Where,

$$t_0 = \left(\frac{\frac{c_1^2}{8} + \sqrt{\frac{c_1^4}{64} + 4(\frac{c_2}{3})^3}}{2} \right)^{1/3} + \left(\frac{\frac{c_1^2}{8} - \sqrt{\frac{c_1^4}{64} + 4(\frac{c_2}{3})^3}}{2} \right)^{1/3} \tag{18}$$

and $a_0 = \sqrt{2t_0}$, $b_0 = \sqrt{t_0^2 + c_2}$. In the case of slow TCs ($l > L_{\mathrm{cr}}$), the wave group only crosses $X = l$ once. The smallest α (which is $\alpha 1$) corresponds to this situation, α_2 corresponds to a non physical solution.

S7.3.2 Fast TCs

If the TC is too fast, wind speed not strong enough and its size too small, then there is no turning point inside the TC where the waves group velocity equal the TC translation speed. Then we have to compute the wave age at the rear of the TC. To get the maximum amount of energy, the generation must start from the front of the TC, in order to travel distance l in the moving frame of reference. Then, we need to solve equation 14 but using $\tilde{X} = \tilde{L_{cr}} - lg/V_{\mathrm{max}}^2$. The equation to solve is the same than 16 but with $c_1 = c_\alpha^4 V_{\mathrm{max}}^2/(lg\alpha_T(1+q))$ and $c_2 = -c_\alpha^4 V_{\mathrm{max}}^2/(lg)$. In this case we consider the largest α (which is α_2), corresponding to the first time the wave group crosses the TC rear. The other solution α_1, corresponds to the second time the wave group crosses the TC rear, after the group velocity have reached the TC referential speed. However it is not physical as we assume there is no wind blowing for $\tilde{X} < L_{\mathrm{cr}} - l$.

S7.3.3 Combination of slow and fast solutions

The two solutions, for slow and fast TCs, can be combined to get the function $\alpha_{\mathrm{min}}(V_{\mathrm{max}}, V_{\mathrm{t}}, R_{\mathrm{max}})$, providing the wave age of the emitted waves depending on the 3 main TC parameters. Using the dispersion relationship in deep water, the peak wavelength can be obtained as function of $(V_{\mathrm{max}}, V_{\mathrm{t}}, R_{\mathrm{max}})$. Similar computations can be performed in the case of waves propagating towards TC rear, using equation 15.

S8 The TC waves multi-sensor product

The TC waves multi-sensor product provides the information on the directional distribution for the wavelength of outrunning swells. A sample corresponding to TC Larry, that illustrates the method in this article, is provided. Information is summarized through two datasets. The "observations dataset" contains all wave acquisitions used to generate the wave roses, and a second one provides the 4 elliptical fit parameters (presented in section 5.3) associated to each tropical cyclone timestamp, such as tropical cyclone track information from the IBTrACS database.

S8.1 Observations dataset

This dataset contains information on wave acquisitions performed outside the TC vortex that were back propagated to be assigned to a TC timestamp for their generation. Variables related to measurements are presented in the table below.

Observation variables	Units	Description
date_obs		Time of measurement
hs_obs	m	Significant wave height measured
wl_obs	m	Wavelength measured
dir_obs	degrees clockwise with respect to North	Direction of propagation measured
lon_obs	degrees	Longitude of measurement
lat_obs	degrees	Latitude of measurement
removed_ambiguity		1 if direction of propagation was changed by 180 degrees to remove the ambiguity, 0 if not
dir_at_TC_generation	degrees clockwise with respect to North	Direction of propagation of the wave system measured when it was generated by the tropical cyclone
wl_obs_ww3	m	Wavelength of the WW3 wave system co-located and assigned to the measurement
dir_obs_ww3	degrees clockwise with respect to North	Direction of propagation of the WW3 wave system co-located and assigned to the measurement
hs_obs_ww3	m	Direction of propagation of the WW3 wave system co-located and assigned to the measurement
spec_dist_obs_ww3	-	Spectral distance between measurement and assigned WW3 wave system
date_generation		Time when the propagated wave system leaves the tropical cyclone
dist_to_TC_center	km	Distance traveled by the wave system between the tropical cyclone (center) and its measurement
TC_hs_ratio	-	Ratio between the significant wave height of the WW3 wave system assigned to the propagated measurement and the total WW3 significant wave heigh, at generation time
sensor_spec		Specification on the sensor used (A or B for Sentinel-1, angle of incidence for SWIM, buoy ID for buoys)
sensor		Sensor used for measurement: S1WVL2 (Sentinel-1 Wave mode Level 2), SWIML2S (CFOSAT SWIM L2S), Spotter_part (Spotter buoys), NDBC (NDBC buoys)
dir_wr_to_TC	degrees clockwise with respect to North	Direction of propagation with respect to TC heading direction, at time of generation

Variables related to back propagation trajectories are described in the table below.

Propagation variables	Units	Description
`date_propag`		Time steps of back propagation trajectory
`lon_propag`	degrees	Longitude of back propagation trajectory
`lat_propag`	degrees	Latitude of back propagation trajectory
`dir_propag`	degrees clockwise with respect to North	Direction of propagation along back propagation trajectory
`hs_propag_ww3`	m	Significant wave height of closest WW3 partition along back propagation trajectory
`hs_total_ww3`	m	Significant wave height of the whole WW3 spectrum along back propagation trajectory
`wl_propag_ww3`	m	Peak wavelength of closest WW3 partition along back propagation trajectory
`dir_propag_ww3`	degrees clockwise with respect to North	Direction of propagation of closest WW3 partition along back propagation trajectory
`spec_dist`		Spectral distance between propagated observation and closest WW3 partition along back propagation trajectory

S8.2 Life cycle dataset

This dataset contains:

- IBTrACS parameters for each timestamp of the cyclone
- If possible the ellipse fit parameters and information regarding the quality of the wave rose and the fit at each TC timestamp

IBTrACS parameters	Units	Description
`time`	date	Date of track steps
`lon`	degrees	Longitude of track steps
`lat`	degrees	Latitude of track steps
`vmax`	m/s	Maximum wind speed
`Rmax`	km	Radius of maximum winds
`translation_speed`	m/s	Translation speed of the cyclone
`translation_direction`	° cw from North	Direction of translation of the cyclone
`curvature`	km	Curvature of the cyclone trajectory (> 0 turning to the right)
`R34`	km	34 kts wind radius
`R50`	km	50 kts wind radius
`R64`	km	64 kts wind radius
rU_*quad*	km	U (64, 50 or 34) kts wind radiuss in quadrant *quad* (ne, se, so, no)
`Lcr`	km	Critical fetch as defined in Kudryavtsev et al. (2015)
`std_vmax`	m/s	Standard deviation of maximum wind speed during last 24 hours
`std_Rmax`	km	Standard deviation of radius of maximum winds during last 24 hours
`std_translation_speed`	m/s	Standard deviation of translation speed during last 24 hours
`std_R34`	km	Standard deviation of R34 during last 24 hours
`d_vmax`	m/s / h	Derivative of maximum wind speed
`d_Rmax`	km / h	Derivative of radius of maximum winds
`d_translation_speed`	m/s / h	Derivative of translation speed
`d_R34`	km / h	Derivative of R34
`TC_atcf_id`		Cyclone ATCF id
`TC_name`		Cyclone name

Ellipse fit parameters	Units	Description
L_el	m	Half major axis for ellipse fit
l_el	m	Half minor axis for ellipse fit
e_el	m	Distance to wave rose center for ellipse fit (front-rear asymetry)
phi0_el	° cw from TC	Orientation of the wave rose for ellipse fit
mean_wavelength_el	m	Mean wavelength of the ellipse fit (L + l) / 2
aspect_ratio_el	-	Aspect ratio of the wave rose defined as 2 l / (L + l)
metric_el	-	wave rose filling for ellipse fit, D parameter described in section 5.3
res_el	m	wave rose residual for ellipse fit, E parameter described in section 5.3
data_reliability_el	1/m	Reliability of ellipse fit (= D / E as defined in section 5.3)

References

CNES, O., Ifremer. (2017, November). *Swim l2s product, algorithm theoretical basis document* (Tech. Rep.). Ifremer Wind and Wave Operational Center.

Engen, G., & Johnsen, H. (1995). Sar-ocean wave inversion using image cross spectra. *IEEE Transactions on Geoscience and Remote Sensing*, *33*(4), 1047-1056. doi: 10.1109/36.406690

Hanson, J. L., Tracy, B. A., Tolman, H. L., & Scott, R. D. (2009). Pacific hindcast performance of three numerical wave models. *Journal of Atmospheric and Oceanic Technology*, *26*(8), 1614–1633.

Houghton, I., Smit, P., Clark, D., Dunning, C., Fisher, A., Nidzieko, N., ... Janssen, T. (2021). Performance statistics of a real-time pacific ocean weather sensor network. *Journal of Atmospheric and Oceanic Technology*, *38*(5), 1047–1058.

Husson, R. (2012). *Développement et validation d'un modèle global de houle basé sur les observations de radar à ouverture synthétique en mode vague* (Unpublished doctoral dissertation). Brest.

Ifremer, E. (2022, August). *Maxss: Storm atlas algorithm theoretical baseline document* (Tech. Rep.). Author.

Knapp, K. R., Kruk, M. C., Levinson, D. H., Diamond, H. J., & Neumann, C. J. (2010). The international best track archive for climate stewardship (ibtracs): Unifying tropical cyclone data. *Bulletin of the American Meteorological Society*, *91*(3), 363 - 376. Retrieved from \url{https://journals.ametsoc.org/view/journals/bams/91/3/2009bams2755_1.xml} doi: 10.1175/2009BAMS2755.1

Kudryavtsev, V., Golubkin, P., & Chapron, B. (2015). A simplified wave enhancement criterion for moving extreme events. *Journal of Geophysical Research: Oceans*, *120*(11), 7538–7558. Retrieved 2022-10-27, from https://onlinelibrary.wiley.com/doi/abs/10.1002/2015JC011284 (_eprint: https://onlinelibrary.wiley.com/doi/pdf/10.1002/2015JC011284) doi: 10.1002/2015JC011284

Kudryavtsev, V., Yurovskaya, M., & Chapron, B. (2021a, April). 2D Parametric Model for Surface Wave Development Under Varying Wind Field in

Space and Time. *Journal of Geophysical Research: Oceans*, *126*. Retrieved from https://onlinelibrary.wiley.com/doi/10.1029/2020JC016915 doi: 10.1029/2020JC016915

Kudryavtsev, V., Yurovskaya, M., & Chapron, B. (2021b). Self-similarity of surface wave developments under tropical cyclones. *Journal of Geophysical Research: Oceans*, *126*(4). Retrieved 2022-10-20, from https://onlinelibrary.wiley.com/doi/10.1029/2020JC016916 doi: 10.1029/2020JC016916

Lygre, A., & Krogstad, H. E. (1986). Maximum entropy estimation of the directional distribution in ocean wave spectra. *Journal of Physical Oceanography*, *16*(12), 2052–2060.

Stopa, J. E., Ardhuin, F., Chapron, B., & Collard, F. (2015). Estimating wave orbital velocity through the azimuth cutoff from space-borne satellites. *Journal of Geophysical Research: Oceans*, *120*(11), 7616–7634.

Young, I., & Burchell, G. (1996). Hurricane generated waves as observed by satellite. *Ocean Engineering*, *23*(8), 761–776.

Young, I., & Vinoth, J. (2013). An "extended fetch" model for the spatial distribution of tropical cyclone wind–waves as observed by altimeter. *Coastal Engineering*, *70*, 14–24. Retrieved 2022-12-16, from https://linkinghub.elsevier.com/retrieve/pii/S0029801813001960 doi: 10.1016/j.oceaneng.2013.05.015

Young, I. R. (1988). Parametric hurricane wave prediction model. *Journal of Waterway, Port, Coastal, and Ocean Engineering*, *114*(5), 637–652.